Mechanical properties and bio-tribological performance of PVD $(Ta/ZrN)_n$ multilayer coatings on UHMWPE in bovine serum lubrication

Chems Eddine Ramoul[1,2] · Corinne Nouveau[3] · Nasser Eddine Beliardouh[2] · Emrullah Hakan Kaleli[4] · Ali Ourdjini[5] · Oualid Ghelloudj[1] · Selman Demirtaş[4] · Amel Gharbi[1] · Kheireddine Bouzid[2]

Abstract

This work investigated the tribological performance of $(Ta/ZrN)_n$ multilayer coatings against ultrahigh molecular weight polyethylene (UHMWPE) material. Three multilayer coatings with different designs were deposited on Ti-6Al-4 V substrate and subjected to wear testing under lubrication of diluted bovine calf serum. The results revealed an improvement in wear resistance of $(Ta/ZrN)_n$ multilayer coatings and low coefficient of friction under an applied load of 1 N. High hardness, excellent biotribological properties, and low residual stresses were obtained in the multilayer coating with the thinnest ZrN as the topmost layer of 100 nm. This work demonstrates that Ta/ZrN multilayers can be promising coatings for prosthesis applications.

Keywords PVD coating · Ta/ZrN · UHMWPE · Wear

1 Introduction

With the average life expectancy of the world's population expected to keep increasing, it is estimated that about 30 million adults currently suffer from osteoarthritis and this number will increase to more than 130 million by 2050 [1]. Osteoarthritis is a type of trauma linked to the degeneration of the joint cartilage due to aging or wear and mostly affects hip and knee joints. Osteoarthritis causes pain and disability and may require the replacement of the dysfunctional natural joints with prostheses. Most articular prostheses commonly used in total hip arthroplasty (THA) are composed of two or more parts, and the materials in contact may be metallic, ceramic, or a polymer component articulating against one another. Commonly used polymeric materials include ultra-high-molecular-weight polyethylene (UHMWPE) and poly-methyl methacrylate (PMMA) whereas metal alloys include austenitic stainless steels, titanium alloys (medical

✉ Chems Eddine Ramoul
rchems@yahoo.com; c.ramoul@crti.dz

Corinne Nouveau
corinne.nouveau@ensam.eu

Nasser Eddine Beliardouh
beliardouh_23@yahoo.fr

Emrullah Hakan Kaleli
kalelih@yahoo.com

Ali Ourdjini
aourdjin@uottawa.ca

Oualid Ghelloudj
o.ghelloudj@crti.dz

Selman Demirtaş
demirtasselman@gmail.com

Amel Gharbi
a.gharbi@crti.dz

Kheireddine Bouzid
kheiro.bouzid@yahoo.fr

[1] Research Center in Industrial Technologies (CRTI), P.O. Box 64, 16014 Cheraga, Algeria

[2] Laboratoire d'Ingénierie des Surfaces (LIS), Université BADJI Mokhtar, Annaba, Algeria

[3] Arts et Metiers Institute of Technology, LABOMAP, Université Bourgogne Franche-Comté, HESAM Université, 71250 Cluny, France

[4] Faculty of Mechanical Engineering, Yıldız Technical University, Istanbul, Turkey

[5] Department of Mechanical Engineering, University of Ottawa, Ottawa, Canada

grade), and cobalt-chromium molybdenum alloys (CoCrMo) owing to their superior mechanical properties, high corrosion resistance, and biocompatibility with the host body.

Degradation and failure of hip and knee joint implants usually occur within about 10 to 15 years of use. Such degradation is essentially caused by the release of wear particles from the polymer (tribology's consequence phenomena) and metal ion release (corrosion's consequence phenomena) into the host body [2]. As a result, biological reactions such as allergy, inflammation, and fever may occur leading to infection of the surrounding tissue, osteolysis, other pathologies, and even aseptic loosening of the implant [3]. It is therefore essential to minimize the release of these debris and metallic ions and enhance wear and corrosion resistance of implant materials. One strategy in dealing with these issues consists of protecting metallic implants by a high corrosion-resistant and biocompatible coating that would reduce the release of wear debris. Several methods are commonly used for the deposition of the protective coatings with physical vapor deposition (PVD) being one of the most common technique employed to extend the service life of implants with promising results [4].

Zirconium, tantalum, and their ceramic alloys are some of the most biocompatible materials commonly used in arthroplasty [5, 6]. Zirconium nitride (ZrN) is currently considered suitable for biomedical implants due to its excellent corrosion resistance, high tensile strength, and good biocompatibility. ZrN coatings reduce bacterial biofilm formation on orthopedic implants and exhibit better tribological properties than titanium nitrides (TiN) [7], which is attributed to its ability to form stable oxide layers [8–10]. Tantalum is another attractive metallic component for use in biomedical applications because it induces minimal adverse biological responses and has outstanding corrosion resistance [11, 12]. García et al. [13] reported that tantalum and zirconium in ternary nitride system coating (TaZrN) deposited by magnetron sputtering onto Ti-6Al-4 V alloy were found to enhance both corrosion resistance and wear resistance.

The use of multilayer coatings alternating between ceramic/metal configurations in biomedical applications has shown an increasing trend due to their improved mechanical and tribological properties [14–16]. Indeed, the combination of hard ceramic and soft metallic phases in multilayer systems reduces internal stresses, provides barriers to dislocation motion, and increases toughness. Moreover, the number and thickness of the coating layers, as well as the thickness ratio of the different layers have a greater effect on the mechanical performance of these coatings [17, 18]. Hernández-Navarro et al. deposited TaZrN/TaZr multilayer PVD coating on AISI-316L stainless steel [19] and observed that the coating exhibited higher hardness and better adhesion performance than TaZrN monolayer coating. Shang et al. [20] compared the mechanical performance of TiN/Ta multilayer coating to TiN monolayer coating and found that the introduction of Ta layer in TiN/Ta multilayer system led to reduced residual stress (72% of the TiN monolayer one) and increased nano hardness (14% higher than that of the TiN monolayer). To the best knowledge of the authors, no research work has been reported on Ta/ZrN multilayer coatings deposited by radio frequency (RF) magnetron sputtering. Therefore, this paper aims to investigate the effects of the bilayer period (some of Ta and ZrN thicknesses) on the tribological performance against UHMWPE polymer in simulated body fluid.

2 Experimental procedure

Thin film specimens were deposited using reactive RF magnetron sputtering (model NORDIKO 3500 system; 13.56 MHz). The deposition was performed simultaneously on silicon Si (100) wafers (10 mm × 10 mm) and Ti-6Al-4 V substrates (diameter $\phi = 11$ mm, 4 mm in thickness, and surface roughness $R_a \leq 0.05$ µm). The deposition of coatings was also performed on pins with a semi-spherical head (radius of curvature = 5.5 mm, 20 mm in length, and $R_a \leq 0.6$ µm).

The Si substrates were used in physicochemical analysis such as X-ray diffraction (XRD), energy dispersive spectroscopy (EDS), and residual stress determination. Cross-section microstructure analysis was carried out on specimens deposited on Si substrates since it is easy to cut the Si wafer transversally using a diamond tip. Ti-6Al-4 V metallic substrates are used in mechanical analysis such as nanoindentation, scratch, and sliding tests (rotating disk) while coated pins are exclusively used in reciprocating sliding tests.

Prior to deposition, the substrates were ultrasonically cleaned with acetone for 10 min, then cleaned with ethanol solution (5 mn per sample) and finally dried in pressurized air. The Zr and Ta targets, having a diameter of 106 mm and 3 mm in thickness, have 99.95% and 99.5% of purity, respectively. The target-substrate distance was kept constant at 80 mm. The deposition chamber was initially pumped down to a residual pressure of about 2×10^{-5} Pa. The substrate surface was first etched for 10 min by high-purity Argon plasma (99.99%) at a pressure of 0.4 Pa before deposition. The ion bombardment is induced by applying a negative bias voltage of − 500 V to the substrates to enhance bombardment throughout, avoid unwanted deposition impurities and native oxides at the surface. The targets were also cleaned under an Ar^+ discharge for 5 min at − 500 V (300 W) and 0.4 Pa. During the deposition, the working pressure was maintained at 0.5 Pa for all experiments. The RF power was 400 W corresponding to a bias voltage of − 900 V on the Ta and Zr targets. The multilayer films were obtained by alternately sputtering Ta and Zr targets. The argon and nitrogen partial

pressures were adjusted, and their flow rates were controlled using MKS flow meters during the deposition process.

All specimens have a Zr under layer (~300 nm) deposited directly on Si and Ti-6Al-4 V substrates to improve the adhesion between the substrate and the film. Based on previous works, Ta layer has poor adhesion to Ti-6Al-4 V substrate as well as the lowest mechanical properties when compared to ZrN, so ZrN was chosen as the topmost layer instead of Ta for all specimens. The specimens were labeled ML1, ML2, and ML3. ML1 specimen consists of a classical design alternating a 400 nm thick ZrN layer on a 100 nm Ta layer giving a constant bilayer period of 500 nm. Specimens ML2 and ML3 have different periods of Ta/ZrN as shown in Fig. 1. The ML2 design consists of a progressive decrease in the bilayer period from the interface (substrate/film) towards the external surface with the topmost layer (ZrN) having 100 nm in thickness. Inversely, ML3 specimen was designed with a progressive increase in the bilayer period. The total thickness of all films was ~3 µm.

The microstructures were analyzed using a scanning electron microscope equipped with energy dispersive spectroscopy (EDS) (model Jeol JSM 7800F) and an atomic force microscope (AFM) (model Nanosurf) operating in contact mode with a scan range of 5×5 µm^2 was used to examine the surface morphologies. The hardness and Young's modulus of the Ta/ZrN multilayer coatings and Ti-6Al-4 V substrate were measured by a nano-indenter (XP MTS) equipped with a continuous stiffness measurement module (CSM) according to ISO 14577–4 [21]. Up to 10 tests were performed on each specimen using a diamond Berkovich tip with a radius of 200 nm and each nanoindentation test was conducted at a maximum load of 14 mN. A constant strain rate of 0.05 s^{-1} was applied during loading with the penetration displacement set to less than 10% of the total coating thickness (only less than 1% in the case of E calculation).

The residual stresses (σ) in the multilayer coatings were calculated using Stoney's equation [22, 23]:

$$\sigma = \frac{E_s}{6(1-v_s)}\frac{h_s^2}{h_f^2}\left(\frac{1}{R}-\frac{1}{R_0}\right) \quad (1)$$

where E_s is the Young's modulus of the substrate (195 GPa), v_s is the Poisson's ratio (0.29) of the substrate, h_s is the thickness of the substrate (380 µm), h_f is the thickness of the film, and R_0 and R are the substrate curvature radii of the uncoated and coated Si (100) wafer. The Si curvatures to calculate the stress are measured using an optical profilometer (WYKO, Veeco-NT1100).

Coating adhesion testing was conducted using a scratch tester (Millennium) equipped with a Rockwell C indenter with a tip diameter of 200 µm to evaluate the adhesion of coating film to the Ti-6Al-4 V substrate. Each specimen is scratched over a distance of 5 mm under a progressive load from 1 to 50 N at a loading rate of 49 N/min. The critical loads and failure mechanisms were determined using an optical microscope. Two critical loads were determined during the scratch test: the lower critical load (L_{c1}) corresponding to the first crack event and the higher critical load (L_{c2}) attributed to the first delamination of the coating with substrate exposure.

Two tribological configurations were used to investigate the tribological properties of the couple $(Ta/ZrN)_n$ multilayer coatings against UHMWPE material as shown in Fig. 2. The first configuration consists of a ball-on-disk set up using a rotative tribometer, in which cylindrical specimens are rotated under fixed UHMWPE balls (Fig. 2a). The ball-on-disk test allows to determine the coefficient of friction (COF) and to estimate the wear rates of the tribopair after a long sliding distance of 1000 m. This result is of great importance in biomaterial characterization, because

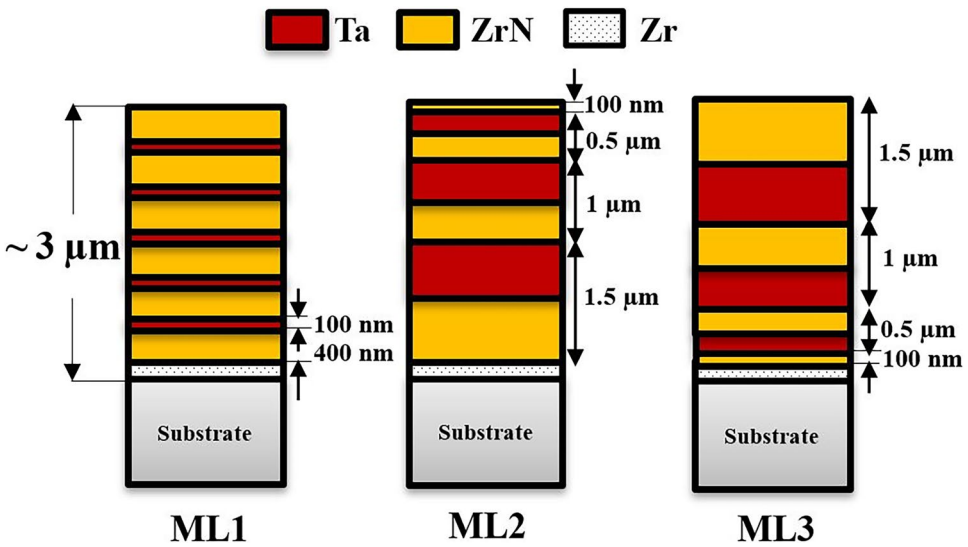

Fig. 1 Scheme of the architecture of the deposited (Ta/ZrN) multilayer coatings

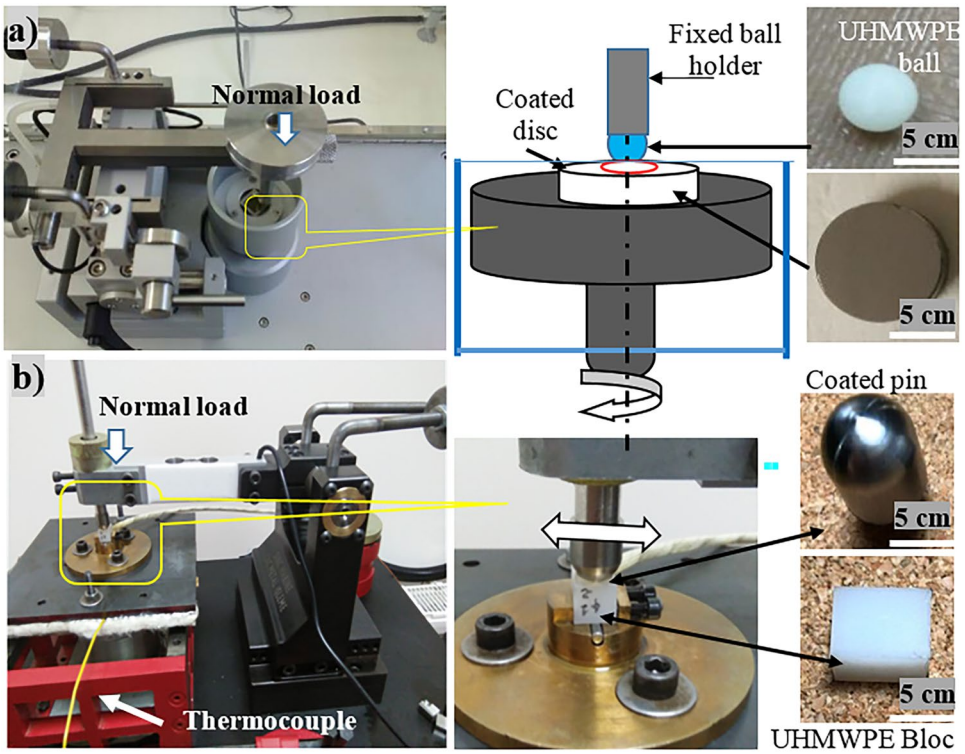

Fig. 2 Tribological test set-ups: **a** ball-on-disk tribometer and **b** pin-on-plate tribometer

releasing of polymer wear debris must be avoided. The second configuration was carried out on a pin-on-plate linear reciprocating tribometer. In this configuration, the pin is made of Ti alloy substrate coated with Ta/ZrN multilayer, taken as the upper counterpart (Fig. 2b), i.e., the moving part, whereas the UHMWPE material, in the form of a cubic block acts as the counterface (fixed part). The pin-on-plate test is a classical test commonly used in biomaterial performance characterization; therefore, special conditions are needed to simulate the human body environment (Table 1). The sliding distance was taken constant (30 min ≈ 18 m sliding distance) for all tests to ensure the COF stabilization.

All the tribological tests were conducted under lubrication of diluted bovine calf serum (BCS; Sigma-Aldrich Ref 12133C) used to simulate the protein concentration closer to that of the human synovial fluid. The lubricant solution was prepared by diluting BCS with deionized water and storing it at a temperature less than − 20 °C and no anti-bacterial agent was used.

Table 1 summarizes the experimental parameters. All experiments were conducted under 1 N of normal applied force, producing a maximum Hertzian contact pressure of 29.3 MPa in the first configuration and 19.6 MPa in the second. The Hertzian maximum contact pressure was calculated according to the following equation:

$$P_0 = \left(\frac{6FE^{*2}}{R^2\pi^3}\right)^{\frac{1}{3}} \quad (2)$$

where F is the normal load (N), R—the ball radius, and E^* is the contact modulus calculated by Eq. (3):

$$\frac{1}{E^*} = \frac{1-\nu_1^2}{E_1} + \frac{1-\nu_2^2}{E_2} \quad (3)$$

where E_1 is the substrate's elastic modulus, E_2 is the UHMWPE ball elastic modulus, and ν_1 and ν_2 are Poisson's ratio of substrate and ball, respectively [24]. The applied forces were chosen based on the Hertz theory for sphere-on-flat contact which is generally used for the total hip prosthesis [25, 26]. The specific wear rate (W_s) of the UHMWPE ball counterpart was calculated using Eqs. (4)–(6).

Table 1 Wear parameters for tests performed in ball-on-disk and pin-on-plate configurations

Parameters	Ball-on-disk	Pin-on-plate
Velocity (cm/s)	10	1
Normal force (N)	1	1
Sliding distance (m)	1000	18
Radius (mm)	4	–
Ball and pin diameter (mm)	6	11
Stroke (mm)	–	8
Temperature (°C)	25 ± 3	37 ± 1
Relative humidity (%)	40 ± 5	40 ± 5

$$W_s = \frac{V}{FL} \tag{4}$$

$$V = \frac{\pi h}{6}\left(\frac{3d^2}{4} + h^2\right) \tag{5}$$

$$h = r - \sqrt{r^2 - \frac{d^2}{4}} \tag{6}$$

where V is the wear volume (mm^3), L is the sliding distance (m), F is the normal load (N), r is the ball diameter, d is the wear scar diameter, and h is the wear depth on the ball.

3 Results and discussion

3.1 Microstructure characterization

The SEM cross-sectional microstructures of the obtained multilayer coatings are shown in Fig. 3a–c exhibiting dense and compact structures. The coating/substrate and Ta/ZrN interfaces appear to be clean and flawless with well-separated ZrN and Ta layers. The corresponding EDS profile for specimen ML2 (Fig. 3b) indicates the expected coating designs. Figure 3d shows that the surface morphology of the ZrN top layer of specimen ML3 exhibits a granular microstructure.

Figure 4 shows the 3D AFM images of the multilayer surface morphologies deposited on the Si substrate, which clearly indicates that all coatings exhibit a relatively smooth surface. Specimen ML3 was found to have the highest grain size (66 ± 1 nm) and a higher surface roughness compared to specimens ML1 and ML2.

3.2 Mechanical properties

Table 2 presents the mechanical properties including hardness and Young's modulus of Ta/ZrN multilayer coatings, surface roughness, and scratch test critical loads. Analysis of the hardness and modulus showed that the hardness value of the coated specimens increased significantly compared to the uncoated specimen. Moreover, when comparing the coated specimens, the results showed that specimen ML1 was found to have the lowest values of hardness and modulus at 14 GPa and 195 GPa, respectively. The influence of compressive residual stresses on the mechanical properties of coatings can be significant. Indeed, the results in Table 2 show that as the compressive stress increases, both hardness and Young's modulus values increased. On the other hand, the ratios of hardness to modulus, H/E and H^3/E^2 are considered to be indicators of the elastic strain to failure and the resistance to plastic deformation, respectively [27]. A higher H^3/E^2 ratio of the coating can lead to the distribution of the applied load over a large area and the hindrance of defect migration [28].

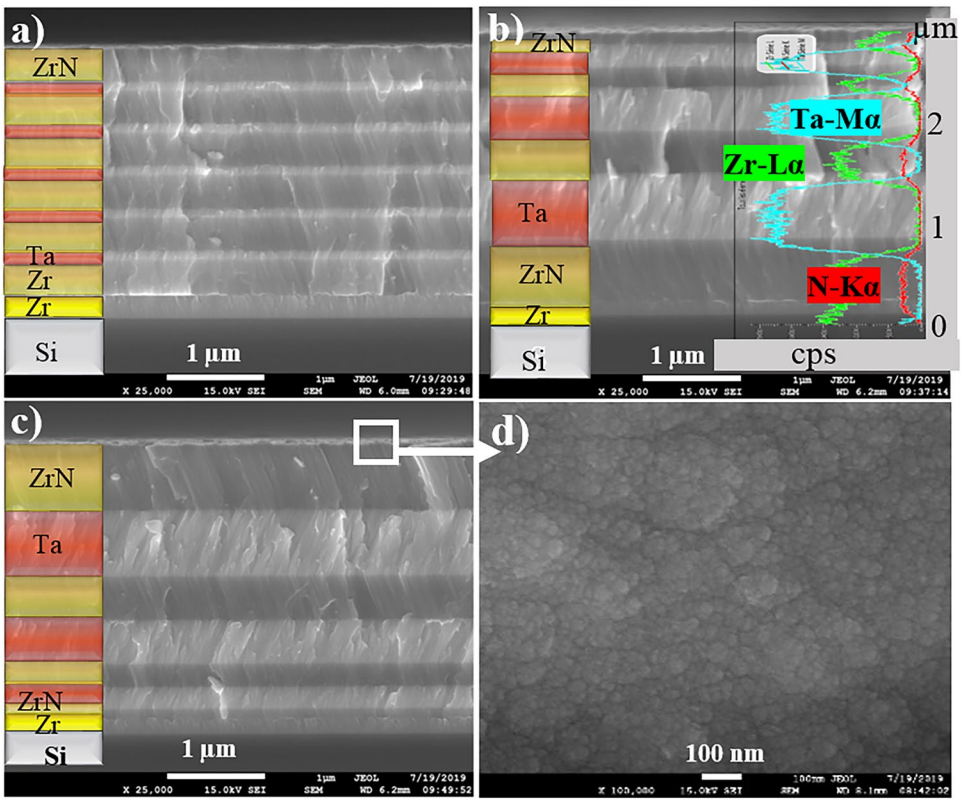

Fig. 3 SEM images of Ta/ZrN multilayer coatings: **a–c** cross-section SEM images of specimens ML1, ML2, and ML3, respectively, **d** surface morphology of the ZrN top layer of ML3

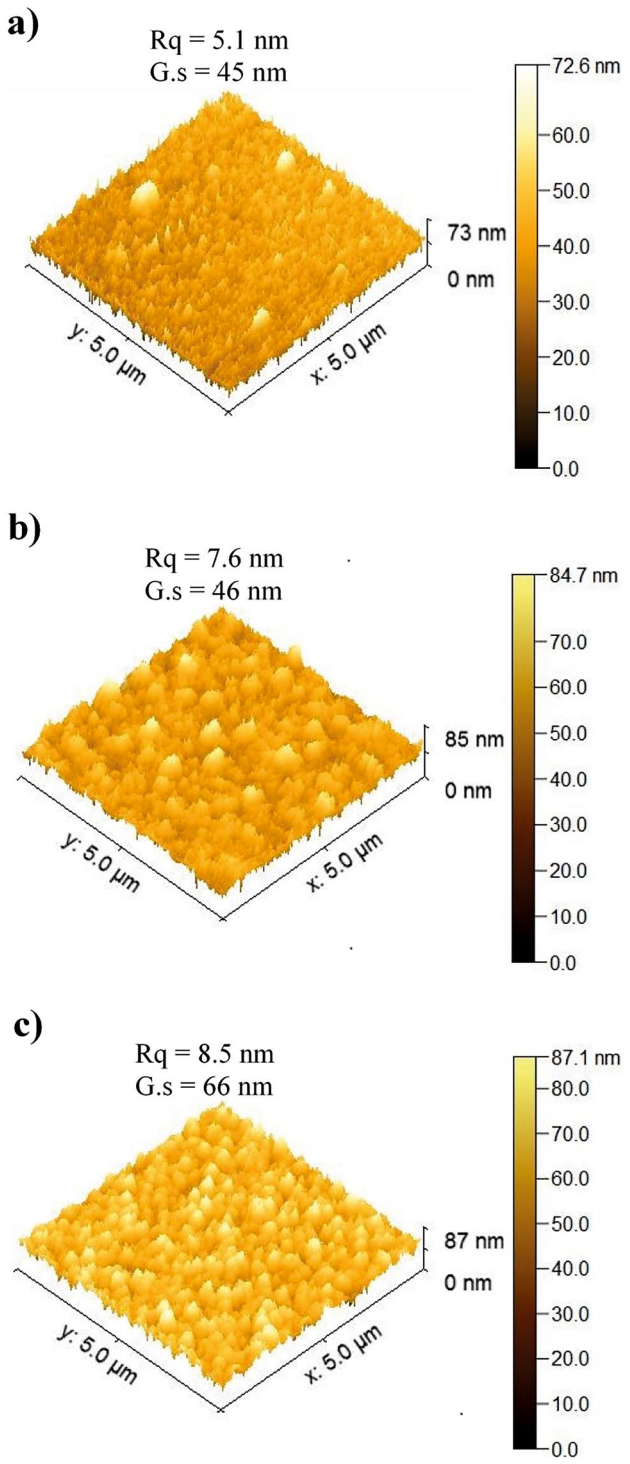

Fig. 4 3-D AFM images of Ta/ZrN multilayers deposited on Si substrate: **a** ML1, **b** ML2, and **c** ML3 specimens

Results in Table 2 show that specimen ML1 has the lowest value of residual stress of − 0.78 GPa and the lowest ratios $H/E = 0.074$ and $H^3/E^2 = 0.08$, while specimen ML2 exhibited the highest values of residual stress and the highest ratios of $H/E = 0.088$ and $H^3/E^2 = 0.15$. It is evident from these results that the designs used for specimens ML2 and ML3 significantly improved the mechanical properties of multilayer coatings.

Adhesion between Ta/ZrN multilayer coatings and the Ti-6Al-4 V substrate was evaluated using scratch testing. The critical loads L_{c1} and L_{c2} correspond to the first crack into the layer and to the first delamination of the coating with substrate exposure, respectively. Results shown in Table 2 indicated that the critical loads are nearly in the same order of magnitude since all the three films have the same underlayer (Zr) at the interface (Zr/Ti-6Al-4 V) as these coatings have been performed in the same conditions (Fig. 1b). Specimen ML1 was found to display the lowest value of adhesion compared to specimens ML2 and ML3.

3.3 Bio-tribological tests

3.3.1 Coefficient of friction

Ball-on-disk testing The tribological results in terms of coefficient of friction (COF) and wear rate obtained from the ball-on-disk testing of multilayer coatings against UHMWPE balls under lubrication of bovine serum at room temperature are shown in Fig. 5. Figure 5a indicates that the coefficient of friction of the uncoated specimen increased almost linearly with increasing sliding distance. The COF decreased in the coated specimens compared to the uncoated substrate and there is a little variation of the coefficient with increasing sliding distance. Specimen ML2 was found to have the lowest average value of the COF (0.08 ± 0.01) while the highest COF of 0.13 ± 0.01 was obtained in specimen ML1 as shown in Fig. 5b.

Figure 5b shows that the highest wear rate of 4.67×10^{-6} $mm^3/N{\cdot}m$ was observed during friction between the polymer ball and specimen ML1 whereas the lowest wear rate was observed against specimen ML2 ($\sim 1.0 \times 10^{-6}$ $mm^3/N{\cdot}m$). It is very important to note that the wear rate (volume loss) values obtained correspond to an extremely long sliding distance (1000 m) to ensure severe conditions. As clearly seen in Fig. 5b, the $(Ta/ZrN)_n$ multilayer coatings resulted in a significant decrease in the wear rate in comparison with the uncoated specimen, with specimen ML2 showing the best improvement. The poor tribological performance of the uncoated substrate is likely attributed to the formation of an oxide layer that may easily produce hard debris, which in turn results in abrasion of the UHMWPE ball during the sliding test. The present results of the wear rate and coefficient of friction of UHMWPE against Ti-6Al-4 V are in good agreement with previous results reported in the literature [29, 30]. The high wear resistance (low wear rate, W_s)

Table 2 Surface characteristics, mechanical properties, and adhesion of the ML1, ML2, and ML3 coatings

	Thickness ± 0.05 (µm)	Roughness		Mechanical properties			Critical loads	
		$R_a \pm 3$ (nm)	$R_q \pm 6$ (nm)	$\sigma \pm 0.1$ (GPa)	$H \pm 1$ (GPa)	$E \pm 5$ (GPa)	$L_{c1} \pm 1$ (N)	$L_{c2} \pm 1$ (N)
ML1	2.9	18	23	− 0.78	14	195	6	17
ML2	2.91	23	29	− 1.17	19	220	10	23
ML3	2.94	29	35	− 1.19	17	206	8	21
Uncoated Ti-6Al-4 V	–	15	19	–	4	125	–	–

observed in specimen ML2 is closely related to its high H/E and H^3/E^2 ratios as shown in Table 2. Indeed, these results are of utmost importance because of the harmful effect of UHMWPE debris on the human body.

Pin-on-plate testing Figure 6 shows the tribological results after reciprocating pin-on-plate tests. The variation of the COF vs. sliding time for the uncoated Ti-6Al-4 V pin and the Ta/ZrN coated pins against UHMWPE blocks is illustrated in Fig. 6a for comparison. It can be seen that all specimens showed similar trend behavior. The COF decreases at the beginning of the test for a short period of time of 150–200 s, corresponding to the running-in period during which the asperities of the pin abrade the polymer surface, and then reaches a steady state. The mean value of the COF was found to be in the range of 0.08–0.13 for all coated specimens. These results are closer to those obtained in the ball-on-disk configuration method described above. The low values of COF displayed by the substrate are not in conflict with the results shown in Fig. 5a since the total test duration is 30 min and corresponds to only about 18 m sliding distance.

The reduction in friction and wear of coated specimens when compared to the uncoated substrate is maybe due to the surface microstructures. It is well known that lubricant viscosity and surface characteristics are principal factors reducing the friction between antagonist pairs. Ti-6Al-4 V alloy instantly forms a thin and brittle oxide film at the top surface which easily generated a great quantity of abrasive debris during rubbing (Fig. 5a) that leads to an increase in the COF evolution. In the case of coated samples, the surface microstructures of ZrN top layer (domes) act as lubricant reservoirs. These lubricant reservoirs are helpful to transport the lubricant to the contact area and form a lubricant film, thus reducing friction [31].

The low COF of specimen ML2 is likely due to the highest resistance to plastic deformation (H^3/E^2) ratio and its good adhesion when compared to ML1 and ML3 specimens. The average arithmetic roughness values (R_a) measured by optical profilometry on the head of pins (top surface) before and after wear testing increase as shown in Fig. 6b. This is evidence of modification of the surface topography, i.e., micro-abrasion by debris generated during sliding pins vs. UHMWPE. EDS microanalysis of the wear debris reveals the presence of elements in contact such as Ta, Zr, C, N, Cl, and O. So, the debris generated during sliding consisted of a mixture of polymer, material from the pin, and oxides. On another hand, it is very difficult to measure precisely the volume loss (wear rate) of the antagonists (pins and UHMWPE blocks). Therefore, only qualitative analysis of wear can be considered. Based on the diagram displayed in Fig. 6b, one can see that ML2 specimen presents the lowest change in surface roughness (ΔR_a), which may indicate that specimen ML2 has the highest wear resistance due to its low COF.

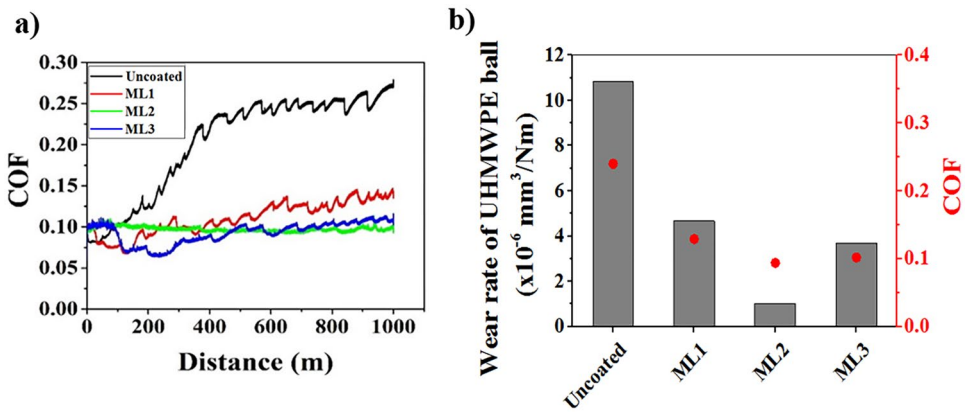

Fig. 5 Ball-on-disk test results: **a** coefficient of friction (COF) evolution vs. sliding distance and **b** calculated specific wear rate of UHMWPE ball and COF average value of uncoated and coated disks

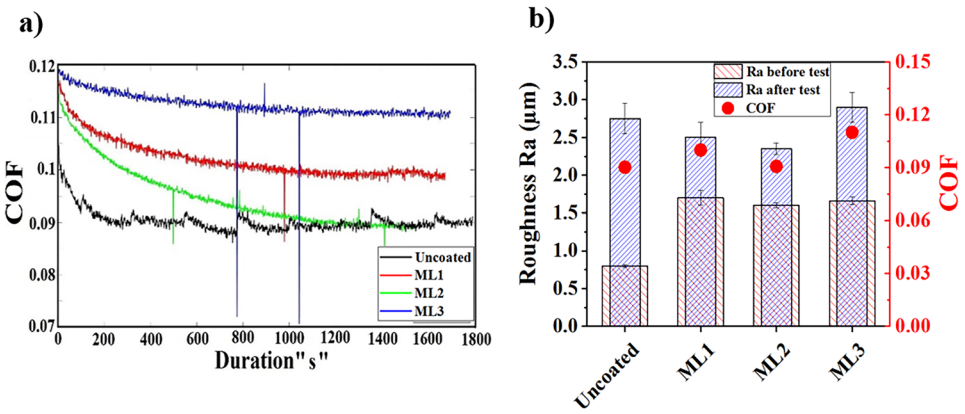

Fig. 6 Reciprocating pin-on-plate test results: **a** coefficient of friction evolutions vs. sliding time and **b** roughness (R_a) before and after tribotests and the mean values of COF

3.3.2 Wear mechanism analysis

Ball-on-disk testing Figure 7 shows SEM images of the wear tracks of disks and optical images of the upper counterface (UHMWPE balls) after 1000 m of sliding distance. The wear track of the uncoated substrate (Fig. 7a) is characterized by furrows parallel to the sliding direction and appears to be the most severely damaged specimen. The EDS spectrum, as shown in Fig. 7b, taken in the middle of the wear track (yellow star in Fig. 7a) confirms the presence of substrate elements (Ti, Al), of oxygen, carbon, and also of elements from the SBF solution (Mg, Ca). The presence of C indicates the transfer of an organic material (UHMWPE polymer) to the disk. Therefore, the main wear mechanism seems to be abrasive wear in addition to adhesive wear.

At the beginning of the sliding test, the wear mechanism involved between the antagonists was essentially mild abrasive wear. With further sliding cycles, the substrate material forms a hard and brittle oxide layer when immersed in the SBF solution. Thus, the wear mechanism transforms into a severe abrasive wear due to the hard debris (oxides) in addition to adhesive wear as clearly indicated by the COF evolution in Fig. 5a.

SEM analysis of wear tracks of the coated specimens revealed fine scratches parallel to the sliding direction indicating abrasive wear in both specimens ML1 (Fig. 7b) and ML3 (Fig. 7d). On the other hand, the limits of the wear track of specimen ML2 (Fig. 7c) are not clearly visible indicating a minimum wear damage. This is another evidence of the high wear resistance of the multilayer ML2 specimen against the UHMWPE ball in bovine serum under the current test conditions. EDS microanalysis (Fig. 7b"–d") of the coated specimens showed the presence of elements from the coating (Ta, Zr, N) and C. Detection of C indicates that some removed material from the UHMWPE ball was transferred to the disk surfaces. The presence of elements such as P, Na, and Mg is attributed to the SBF solution "glued" to the surface specimens during the sliding test. The high "O" peak is probably the result of contamination of the chemical composition of coatings during the sputtering process. There are always a few quantities (less than 5 at.% in this case) of oxygen in PVD sputtering method.

The corresponding optical images shown in Fig. 7a'–d' reveal wear scars on the UHMWPE balls. As seen in the inset of Fig. 7c', the smallest surface scar was observed in the ball that was in contact with specimen ML2 confirming the results of minimum wear rate shown in Fig. 6b between ML2 specimen against UHMWPE ball. Consequently, the coated specimen seems to suffer only mild abrasive and adhesive wear.

Pin-on-plate tests SEM images of the worn surface pins after reciprocating tribotests in bovine serum at 37 °C for 1800s, which is about 18 m sliding distance, are shown in Fig. 8. The worn surface of the uncoated pin only shows some isolated scratches caused by hard debris, most likely oxides. Results of EDS microanalysis show the presence of carbon in addition to the substrate's elements which confirms the results obtained previously in Fig. 7a–a"; abrasive and adhesive wear occurred simultaneously during sliding of the metallic substrate (Ti-6A-4 V) against the UHMWPE material regardless of the configuration. In the case of the coated pins, EDS microanalysis reveal the presence of elements from the coating (Ta, Zr, and N) and elements from the SBF solution (Na, P, and Ca…) but no C was detected (Fig. 8c, e, and i). The fact that no C was detected means that no transfer of polymer material occurred in contrast to the ball-on-disk testing. The worn surfaces of the UHMWPE blocks shown in Fig. 8d, f, and j exhibited plastic deformation regions and few scratch marks (white arrow in Fig. 8b) parallel to the sliding direction. No wear damage was observed on the coated pins. Similar results of wear mechanism of UHMWPE have been observed by Qiufeng et al. [32].

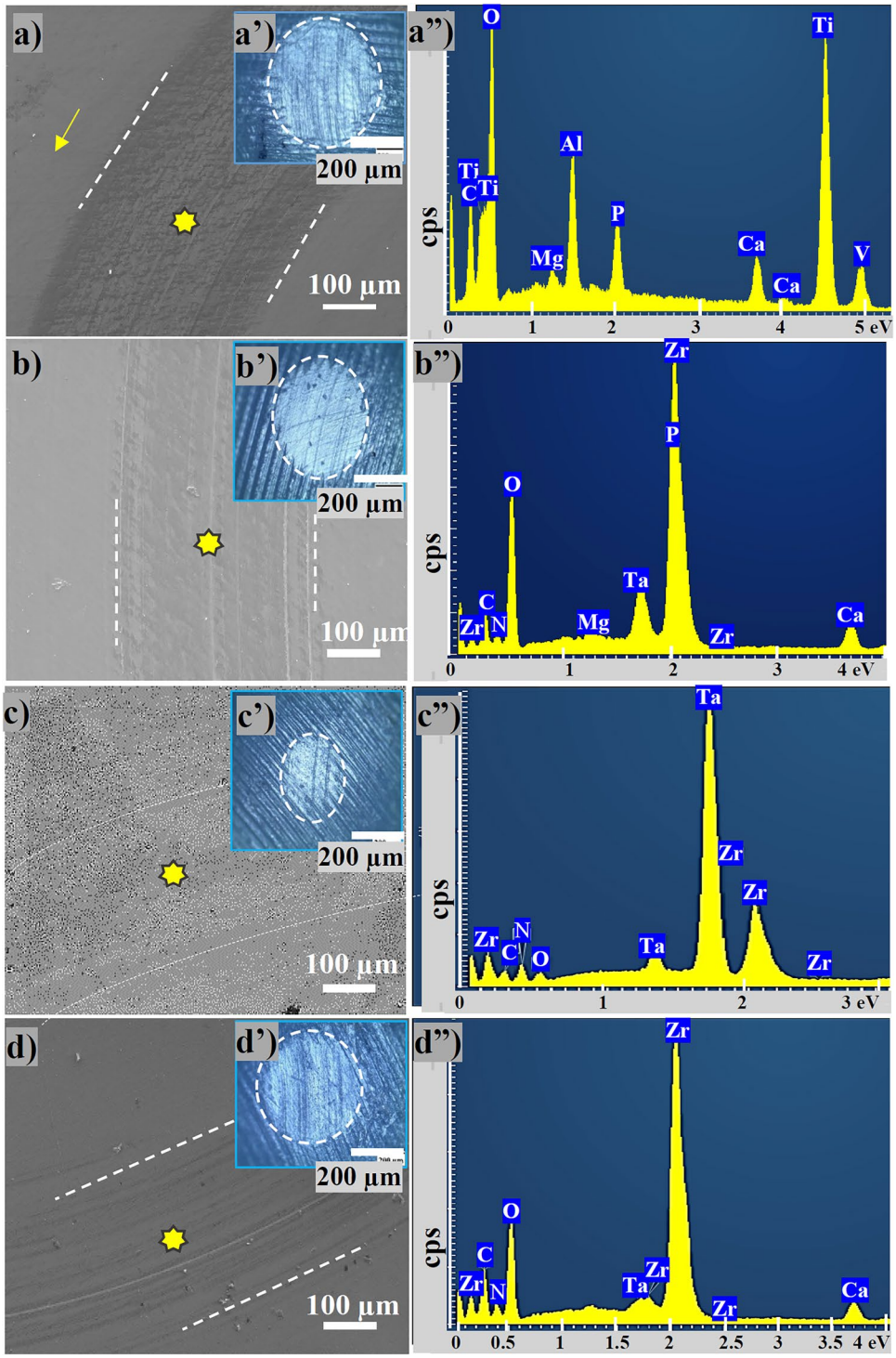

Fig. 7 SEM images, EDS microanalysis of samples, and optical images of the UHM-WPE ball after ball-on-disk testing for (**a**–**a”**) uncoated, (**b**–**b”**) ML1 coated, (**c**–**c”**) ML2 coated, and (**d**–**d”**) ML3 coated Ti-6Al-4 V disks

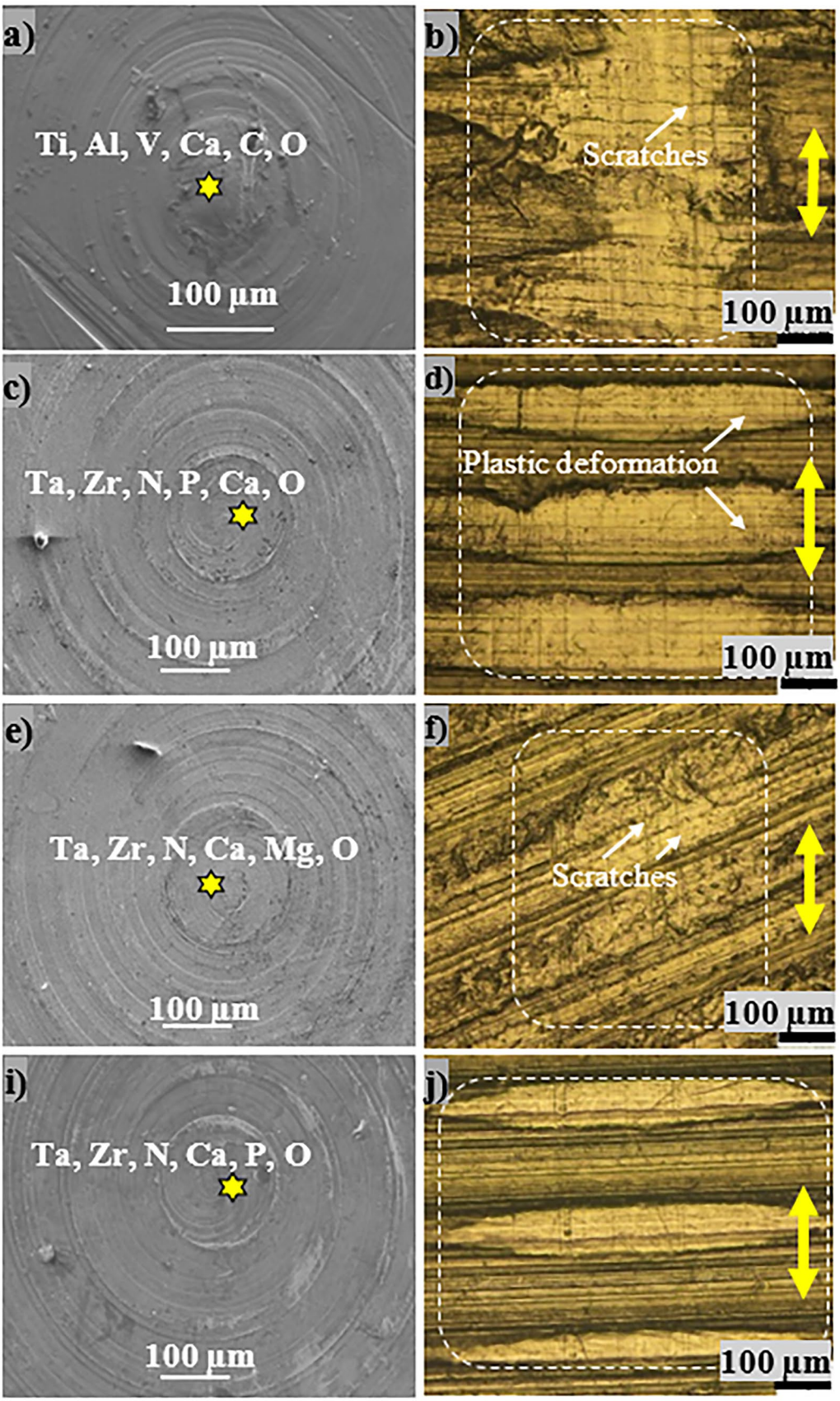
a)
Ti, Al, V, Ca, C, O
100 µm
b)
Scratches
100 µm
c)
Ta, Zr, N, P, Ca, O
100 µm
d)
Plastic deformation
100 µm
e)
Ta, Zr, N, Ca, Mg, O
100 µm
f)
Scratches
100 µm
i)
Ta, Zr, N, Ca, P, O
100 µm
j)
100 µm

◂**Fig. 8** SEM micrographs with EDS analysis results of pins and the corresponding optical images of the counterface UHMWPE blocks, after pin-on-plate tests in bovine serum at 37 °C: **a**, **b** uncoated pin, **c**, **d** ML1, **e**, **f** ML2, and **I**, **j** ML3 specimens

4 Conclusions

Multilayer coatings Ta/ZrN were deposited by RF magnetron sputtering process on Ti-6Al-4 V substrates with three different designs. The wear resistance in bovine serum at 37 °C was evaluated using two different tribotest configurations of ball-on-disk and pin-on-plate. The following conclusions were drawn:

- The multilayer coating with the thinnest ZrN of 100 nm (specimen ML2) was found to have the lowest coefficient of friction and wear rate due to its high H/E and H^3/E^2 ratios. The main wear mechanism involved was third body abrasive wear while the counter face suffered severe abrasive wear in addition to adhesive wear.
- The linear reciprocating pin-on-plate wear test configuration confirms the superior bio-tribological performance of specimen ML2. No wear damages were observed on this coated pin while the polymer counterface of UHMWPE blocks suffered plastic deformation and release of debris.
- The bovine serum does not provide any lubrication effect on the contact pairs investigated in the present work but appears to only reduce the friction forces regardless of the tribological configuration.

Acknowledgements The authors would like to thank the Ministry of Higher Education and Scientific Research of Algeria, MESRS, and DGRSDT for supporting this work (PNR program 2019-2022). The authors would also like to thank the MSMP of ENSAM Lille for their assistance in the nanoindentation and scratch testing and Mr. Denis Lagadrillere for assistance on SEM/EDS analysis.

Author contribution Chems Eddine Ramoul: investigation, data curation, writing - original draft and editing. Corinne Nouveau: conceptualization, supervision, review and editing. Nasser Eddine Beliardouh: supervision, writing - review and editing. Hakan Kaleli: conceptualization, supervision, review. Ali Ourdjini: writing - review and editing. Oualid Ghelloudj: writing - review and editing. Selman Demirtaş: investigation, data curation. Amel Gharbi: resources. Kheireddine Bouzid: investigation, data curation.

Declarations

Ethics approval and consent to participate Not applicable.

Consent for publication Not applicable.

Conflict of interest The authors declare no competing interests.

References

1. Maiese K (2016) Picking a bone with WISP1 (CCN4): new strategies against degenerative joint disease. J Transl Sci 1:83–85. https://doi.org/10.15761/JTS.1000120
2. Liu S, Hall DJ, Della-Valle CJ, Walsh MJ, Jacobs JJ, Pourzal R (2020) Simultaneous characterization of implant wear and tribocorrosion debris within its corresponding tissue response using infrared chemical imaging. Biotribology 26:100163. https://doi.org/10.1016/j.biotri.2021.100163
3. Bahi R, Nouveau C, Beliardouh NE, Ramoul CE, Meddah S, Ghelloudj O (2020) Surface performances of Ti-6Al-4V substrates coated PVD multilayered films in biological environments. Surf Coat Technol 385:125412. https://doi.org/10.1016/j.surfcoat.2020.125412
4. Ortega-Saenz JA, Alvarez-Vera M, Hernandez-Rodriguez MAL (2013) Biotribological study of multilayer coated metal-on-metal hip prostheses in a hip joint simulator. Wear 301:234–242. https://doi.org/10.1016/j.wear.2013.01.024
5. Ramoul C, Beliardouh NE, Bahi R, Nouveau C, Djahoudi A, Walock MJ (2019) Surface performances of PVD ZrN coatings in biological environments. Tribol - Mater Surfaces Interfaces 13:12–19. https://doi.org/10.1080/17515831.2018.1553820
6. Xu G, Shen X, Hu Y, Ma P, Cai K (2015) Fabrication of tantalum oxide layers onto titanium substrates for improved corrosion resistance and cytocompatibility. Surf Coat Technol 272:58–65. https://doi.org/10.1016/j.surfcoat.2015.04.024
7. Pejaković V, Totolin V, Göcerler H, Brenner J, Ripoll MR (2015) Friction and wear behaviour of selected titanium and zirconium based nitride coatings in Na2SO4 aqueous solution under low contact pressure. Tribol Int 91:267–273. https://doi.org/10.1016/j.triboint.2015.04.047
8. Pilz M, Staats K, Tobudic S, Assadian O, Presterl E, Windhager R, Holinka J (2019) Zirconium nitride coating reduced Staphylococcus epidermidis biofilm formation on orthopaedic implant surfaces: an in vitro study. Clin Orthop Relat Res 477:461–466. https://doi.org/10.1097/CORR.0000000000000568
9. Cui W, Cheng J, Liu Z (2019) Bio-tribocorrosion behavior of a nanocrystalline TiZrN coating on biomedical titanium alloy. Surf Coat Technol 369:79–86. https://doi.org/10.1016/j.surfcoat.2019.04.036
10. Kumar DD, Kumar N, Kalaiselvam S, Dash S, Jayavel R (2015) Substrate effect on wear resistant transition metal nitride hard coatings: microstructure and tribo-mechanical properties. Ceram Int 41:9849–9861. https://doi.org/10.1016/j.ceramint.2015.04.059
11. Yang C, Li J, Zhu C, Zhang Q, Yu J, Wang J, Wang Q (2019) Advanced antibacterial activity of biocompatible tantalum nanofilm via enhanced local innate immunity. Acta Biomater 89:403–418. https://doi.org/10.1016/j.actbio.2019.03.027
12. Rahmati B, Sarhan AAD, Basirun WJ, Abas WABW (2016) Ceramic tantalum oxide thin film coating to enhance the corrosion and wear characteristics of Ti-6Al-4V alloy. J Alloys Compd 676:369–376. https://doi.org/10.1016/j.jallcom.2016.03.188
13. Garcia E, Flores M, Rodriguez E, Rivera LP, Camps E, Muhl S (2018) Tribological, tribocorrosion and wear mechanism studies of TaZrN coatings deposited by magnetron sputtering on TiAlV alloy. Coatings 8:295. https://doi.org/10.3390/coatings8090295
14. Shanaghi A, Ghasemi S, Chu PK (2018) Improving of tribology properties of TiAl6V4 with nanostructured Ti/TiN multilayered coating deposited by high-vacuum magnetron sputtering. Appl Phys A 124:822. https://doi.org/10.1007/s00339-018-2221-1
15. Shugurov AR, Kazachenok MS (2018) Mechanical properties and tribological behavior of magnetron sputtered TiAlN/TiAl

multilayer coatings. Surf Coat Technol 353:254–262. https://doi.org/10.1016/j.surfcoat.2018.09.001
16. Majora L, Krawiec H, Lackner J, Dyner M, Grysakowski B, Majo B (2020) Nanoscale characterization of corrosion mechanisms in advanced Zr/ZrxN and Zr/ZrxN+a-C:H nano-multilayer coatings for medical tools. Mater Charact 168:110565. https://doi.org/10.1016/j.matchar.2020.110565
17. Ali R, Sebastiani M, Bemporad E (2015) Influence of Ti-TiN multilayer PVD-coatings design on residual stresses and adhesion. Mater Des 75:47–56. https://doi.org/10.1016/j.matdes.2015.03.007
18. Guo Z, Ma D, Zhang X, Li J, Feng J (2019) Preparation and toughening of a-CuZr/c-ZrN nano-multilayer hard coatings. Appl Surf Sci 483:432–441. https://doi.org/10.1016/j.apsusc.2019.03.289
19. Hernández-Navarro C, Flores-Martínez M, Camps E, Rivera-Reséndiz LP, Garcia E (2021) Analysis of the wear behavior of multilayer coatings of TaZrN/TaZr produced by magnetron sputtering on AISI-316L stainless steel. Int J Adv Manuf Technol 117:1565–1573. https://doi.org/10.1007/s00170-021-07655-6
20. Shang H, Li J, Shao T (2014) Mechanical properties and thermal stability of TiN/Ta multilayer film deposited by ion beam assisted deposition. Adv Mater Sci Eng 1–2:1–8. https://doi.org/10.1155/2014/639461
21. ISO (2016) 14577–4 metallic materials - instrumented indentation test for hardness and materials parameters - part 4: test method for metallic and non-metallic coatings. Second Edi, International Standard
22. Bouaouina B, Besnard A, Abaidia SE, Airoudj A, Bensouici F (2018) Correlation between mechanical and microstructural properties of molybdenum nitride thin films deposited on silicon by reactive R.F. magnetron discharge. Surf Coat Technol 333:32–38. https://doi.org/10.1016/j.surfcoat.2017.10.028
23. Aissani L, Alhussein A, Nouveau C, Radjehi L, Lakdhar I, Zgheib E (2019) Evolution of microstructure, mechanical and tribological properties of vanadium carbonitride coatings sputtered at different nitrogen partial pressures. Surf Coat Technol 374:531–540. https://doi.org/10.1016/j.surfcoat.2019.06.034
24. Broitman E, Macdonald W, Hellgren N, Radnóczi G, Czigány Z, Wennerberg A, Jacobsson M, Hultman L (2000) Carbon nitride films on orthopedic substrates. Diam Relat Mater 9:1984–1991. https://doi.org/10.1016/S0925-9635(00)00352-6
25. Johnson KL (1985) Contact mechanics. Cambridge University Press, Cambridge. https://doi.org/10.1017/CBO9781139171731
26. Alemón B, Flores M, Ramírez W, Huegel JC, Broitman E (2015) Tribocorrosion behavior and ions release of CoCrMo alloy coated with a TiAlVCN/CN x multilayer in simulated body fluid plus bovine serum albumin. Tribol Int 81:159–168. https://doi.org/10.1016/j.triboint.2014.08.011
27. Leyland A, Matthews A (2000) On the significance of the H/E ratio in wear control: a nanocomposite coating approach to optimised tribological behaviour. Wear 246:1–11. https://doi.org/10.1016/S0043-1648(00)00488-9
28. He N, Li H, Ji L, Liu X, Zhou H, Chen J (2016) High temperature tribological properties of TiAlSiN coatings produced by hybrid PVD technology. Tribol Int 98:133–143. https://doi.org/10.1016/j.triboint.2016.02.034
29. Guezmil M, Bensalah W, Mezlini S (2016) Tribological behavior of UHMWPE against TiAl6V4 and CoCr28Mo alloys under dry and lubricated conditions. J Mech Behav Biomed Mater 63:375–385. https://doi.org/10.1016/j.jmbbm.2016.07.002
30. Xiong D, Gao Z, Jin Z (2007) Friction and wear properties of UHMWPE against ion implanted titanium alloy. Surf Coat Technol 201:6847–6850. https://doi.org/10.1016/j.surfcoat.2006.09.043
31. Hao H, Sun P, Xiao S, Yang Y, Li L (2020) Tribological performance of surface with different wettability under ball-on-disc test. Appl Surf Sci 501:144228. https://doi.org/10.1016/j.apsusc.2019.144228
32. Qiufeng W, Wang Y, Wang H, Fan N, Yan F (2017) Fretting wear behavior of UHMWPE under different temperature conditions. J Macromol Sci Part B Phys 56:493–504. https://doi.org/10.1080/00222348.2017.1330131